Xi et al. Journal of Translational Medicine (2025) 23:266
https://doi.org/10.1186/s12967-025-06270-3

Journal of Translational Medicine

RESEARCH Open Access

Super-enhancer-hijacking RBBP7 potentiates metastasis and stemness of breast cancer via recruiting NuRD complex subunit LSD1

Yuanyin Xi[1†], Ruoding Wang[2†], Man Qu[1†], Qinwen Pan[1], Minghao Wang[1], Xiang Ai[3], Zihan Sun[4], Chao Zhang[5], Peng Tang[1*], Jun Jiang[1*] and Ying Hu[1*]

Abstract

Background Aberrant epigenetic and transcriptional events that drive cancer progression could be precisely targeted. We aimed to uncover the epigenetic roles of RBBP7 on breast cancer (BCa) stemness and metastasis.

Methods The bioinformatic analysis was used to assess the clinical significance of RBBP7 in BCa. CCK8, colony formation, and Transwell assays were utilized to estimate the oncogenic functions of RBBP7. The ChIP-qPCR and dual-luciferase reporter assays were used to investigate the epigenetic mechanisms of RBBP7. Tumor sphere formation assays were conducted to assess the self-renewal abilities of BCa cells. Tail vein injection models were constructed to assess the in vivo metastatic efficiency of BCa cells. The PDOs and PDX models were used to assess the clinical significance of ORY-1001 in suppressing BCa.

Results Here, we found that RBBP7 is upregulated in BCa and associated with poor prognosis. Functional experiments demonstrated that RBBP7 enhanced BCa proliferation and distal metastasis. Mechanistically, a novel RBBP7-super-enhancer (SE) was identified using multiple databases in BCa. RBBP7-SE sustained high levels of RBBP7 and CRISPR/Cas9-mediated deletion of SE decreased RBBP7 levels and suppressed BCa malignant features. Further, our data showed that RBBP7 may correlate with stemness pathway and significantly potentiated BCa cancer stem-like properties. Additionally, RBBP7 interacts with LSD1 and relies on LSD1 to erase suppressive H3K9me3 markers in promoters of downstream stemness targets (SOX9/SOX2/OCT4/CCND1). Thus, RBBP7 recruits LSD1 to transcriptionally upregulate the expressions of key stemness genes, and promote tumor stemness capacity. Pharmacological inhibition of LSD1 by ORY-1001 effectively repressed RBBP7-high BCa tumor growth, stemness properties, and distant metastasis.

†Yuanyin Xi, Ruoding Wang and Man Qu contributed equally to this work.

*Correspondence:
Peng Tang
tp1232000@sina.com
Jun Jiang
jcbd@medmail.com.cn
Ying Hu
yinghu@tmmu.edu.cn

Full list of author information is available at the end of the article

Conclusions Together, our results establish that the SE-RBBP7-LSD1 axis represents a potential therapeutic target for BCa treatment.

Keywords RBBP7, Super-enhancer, Stemness, Metastasis, LSD1

Introduction

As a severe public issue worldwide, breast cancer (BCa) accounts for 30% of all malignancies in women, leading to nearly 15% of female cancer-related deaths. The estimated new cases and deaths caused by BCa in 2024 would reach up to 313,510, and 42,790, respectively [1]. So far, BCa can be commonly categorized into four subtypes, including Luminal A/B, HER2-positive, and triple-negative breast cancer (TNBC). Considering that BCa is a highly heterogeneous disease, BCa patients within different subtypes may show various clinical behaviors and drug responses [2]. The current main strategies for BCa include surgery, radiotherapy, chemotherapy, targeted therapy, hormone therapy, and immunotherapy. However, the intrinsic and acquired drug resistance markedly impaired the efficacy of the above therapies, and a majority of advanced BCa patients suffer from distant metastases [3]. As a result, clarification of the underlying molecular mechanisms of BCa is crucial to finding novel therapeutical targets or predictive biomarkers.

Epigenetic alterations or reprogramming are essential drivers of tumor initiation and progression in BCa [4, 5]. Without altering the genetic contexts, epigenetic mechanisms participate in multiple processes of tumor growth, including gene transcription, genomic stability, or cell differentiation [6]. Therefore, epigenetics-based diagnostic and prognostic management significantly contributes to precision oncology, especially in BCa. As reported, the Retinoblastoma gene (Rb) encodes retinoblastoma protein (pRb) that modulates multiple biological events via unique epigenetic processes [7]. The retinoblastoma-binding protein (RBBP) family contains a specific domain to interact with pRb and attracts attention owing to its specific epigenetic roles. Among these RBBP family members, RBBP4 and RBBP7 constitute several well-known epigenetic complexes that mediate histone modifications or chromatin remodeling, including polycomb repressive complex 2 (PRC2), nucleosome remodeling and deacetylase (NuRD) and nucleosome remodeling factor (NURF) [8, 9]. Aberrant RBBP7 mutations or expression levels highly correlate with multiple tumorigenesis. For instance, a deleterious hemizygous variant of X-linked RBBP7 was identified to drive the development of Leydig cell tumors [10]. Furthermore, RBBP7, induced by SP1, could elevate glycolysis-related genes to promote aerobic glycolysis in liver cancer [11]. Meanwhile, in 2020, Jianqing Wang et al. revealed that RBBP7 could also interact with HNF1B to suppress the EMT process by repressing SLUG expression in prostate cancer, implicating that RBBP7 can also exert tumor-suppressive functions [12]. In line with previous statistical studies, reverse transcription-PCR data show high expressions of RBBP7 in 79% of breast carcinoma cases, which is likely to have a role in the development or progression of BCa [13]. The Cancer Genome Atlas (TCGA) pan-cancer analysis further implicated that RBBP7 is highly expressed in BCa, relative to other tumor types. However, limited studies clearly defined the underlying mechanisms by which RBBP7 influences BCa progression.

Cancer stem cells (CSCs) refer to self-renewing cells capable of generating heterogeneous cancer cells, accounting for the proliferation, metastasis, and relapse of cancer. Besides, conventional strategies for BCa failed to eliminate all tumor cells, largely due to the existence of breast CSCs (BCSC) that caused recurrence and drug resistance [14]. Tumor stemness and metastasis are commonly coupled and coordinate with each other to drive cancer progression. Disseminated cancer cells normally need to obtain self-renewal capability to enter the circulatory system, rooting a new microenvironment and spawning macroscopic metastases [15, 16]. Therefore, tumors containing a higher proportion of the self-renewal population usually spread more widely. Nevertheless, the intrinsic mechanisms for the progression of cancer stemness and metastasis abilities, as well as the underlying relationships between the two phenotypes, are poorly understood in BCa. Currently, emerging evidence demonstrates that epigenetic events may play an important role in BCa stemness maintenance. Histone reader ZMYND8 increased the stability of NRF2 to potentiate BCSC stemness and tumor initiation via inhibiting ROS and ferroptosis [17]. Consistently, transcriptional complex negative elongation factor (NELF) cooperates with KAT2B to promote the expression of epithelial-mesenchymal transition (EMT) and stemness-associated signature in breast cancer [18]. Several drugs or small-molecular epigenetic inhibitors were discovered and validated to inhibit CSCs, including GSK591, JQ1, or THZ1 [19–21]. Based on our previous data, we hypothesized that RBBP7 may participate in transcriptional regulations to drive the growth of BCSC. Thus, targeting RBBP7 may serve as an effective method to destroy transcriptional machinery for suppressing cancer stemness or initiation.

Here, in the present study, we confirmed that high RBBP7 levels correlated with poor outcomes in BCa patients. Oncogenic roles of RBBP7 in BCa were thoroughly validated by functional experiments. High RBBP7,

driven by a BCa-specific super-enhancer, could recruit LSD1 to activate a series of stemness-related genes. Our study highlights that RBBP7-LSD1 may serve as a novel complex to determine BCSC survival and proliferation, endowing an attractive epigenetic vulnerability for BCa treatment.

Methods and materials

Cell culture

Human breast cancer cell lines (MCF-7, T-47D, ZR-75-1, MDA-MB-231, MDA-MB-453, and HS-578T) and normal breast epithelial cell line MCF-10 A were purchased from America Type Culture Collection (ATCC, Manassas, USA) and cultured with Dulbecco's modified Eagle medium (DMEM) containing 10% fetal bovine serum (FBS, Gibco, USA) and 100 U/ml penicillin/streptomycin (ThermoFisher Scientific, USA). All Cells were cultured in a humidified incubator with 5% CO_2 at 37 °C.

Cell transfection

Cells were transfected with plasmid DNA or siRNA RNA duplexes by Lipofectamine 2000 (Invitrogen) according to the manufacturer's protocol. In transient transfection experiments, plasmid DNA was kept constant with an empty vector. shRNAs were delivered by lentiviral infection with lentiviruses produced by transfection of HEK293T cells with the vector pLKO.1. Cells infected with lentiviruses delivering scrambled shRNA (shCtrl) were used as negative control cells. Short interfering RNA (siRNA) sequences were directly synthesized (GenePharma, Shanghai, China). The sequences of shRNAs and siRNAs are listed as the following: **shRNA**: RBBP7(5'->3'):F: CCGGCGTGTCATCAATGAAGAATATCTCGAGATATTCTTCATTGATGACACGTTTTTG, R:AATTCAAAAACGTGTCATCAATGAAGAATATCTCGAGATATTCTTCATTGATGACACG. LSD1(5'->3'):F: CCGGCCAACAATTAGAAGCACCTTACTCGAGTAAGGTGCTTCTAATTGTTGGTTTTTG, R:AATTCAAAAACCAACAATTAGAAGCACCTTACTCGAGTAAGGTGCTTCTAATTGTTGG. **siRNA**: RBBP7(5'->3'): GCGGATAAGACCGTAGCTTTA; LSD1(5'->3'): GCCTAGACATTAAACTGAATA; HDAC1(5'->3'): GCTGCTCAACTATGGTCTCTA; MTA1(5'->3'): AGACATCACCGACTTGTTAAA; MTA2(5'->3'): CCAGCAATCCTTACCTGGTTA; p300(5'->3'): GCCTTCACAATTCCGAGACAT.

MTT assay and colony formation

The Cell Counting Kit-8 (Beyotime, Shanghai, China), colony formation, and 5-ethynyl-2-deoxyuridine (EdU, Beyotime, Shanghai, China) assays were performed as described previously [22]. Proliferation was analyzed using the mean number of cells in three fields for each sample. For the colony formation assays, For colony formation assay, shRNA-treated BRCA cell lines MCF-7 and T-47D were coated into 6-well plates with 5×10^5 and 1×10^5 cells, respectively. Five repetitions were used in each group. After 14-day incubation, these plates were washed with phosphate buffered saline (PBS) twice, fixed with methanol for 10 min, and stained with 0.1% crystal violet solution within 10 min for further analysis.

Transwell and scratch wound healing assay

Transwell assays using Boyden chambers containing 24-well Transwell plates (BD Inc., USA) with 8 mm pore size were used to evaluate the migration and invasiveness of cells. All experiments were performed in duplicate and repeated three times. For the migration assay, the cell culture inserts were seeded with 1×10^5 (MCF-7,T-47D cells) or 2×10^4 (MDA-MB-231 cells) in 100mL of serum-free culture medium without an extracellular matrix coating. A culture medium containing 10% FBS was added to the bottom chamber. After 20 h of incubation, the cells on the lower surface of the filter were fixed, stained, and examined using a microscope. For the invasion assay, the membrane was coated with 50 mL of 1:8 diluted Matrigel (BD Biosciences, USA). After the Matrigel had solidified at 37 °C for 2 h, cells were added to the cell culture, whereas the lower chamber was filled with culture medium containing 20% FBS. The Boyden chamber was then incubated at 37 °C in 5% CO2 for 24 h. The cells were then stained and observed as described for the migration assays. For the wound healing assays, transfected MCF-7 or MDA-MB-231 were seeded into six-well plates and cultured until 90% confluence. An artificial wound was created using a sterile 200 μL tip. The floating cells were washed away using PBS and the remaining cells were cultured in a serum-free medium for 48 h. The wound was recorded by an inverted microscope and cell migration was calculated.

Chromatin Immunoprecipitation (ChIP) analysis

For the chromatin immunoprecipitation (ChIP) experiment, 1×10^5 MCF-7 cells were treated with 1% formaldehyde at room temperature for 10 min to crosslink chromatin proteins to DNA. Then a final concentration of 0.125 M glycine was added to the dish for 5 min to terminate the crosslink. Cells were lysed in a lysis Buffer (50 mM Tris-HCl pH 8.0, 0.5 mM EDTA, 1% SDS, and protease inhibitors) and the resulting lysate was sonicated to break chromatin into fragments with an average length of 300 ~ 500 bp, followed by immunoprecipitation with anti-RBBP7 or anti-LSD1 antibody and purification of immunoprecipitated DNA fragments. PCR was then performed with the following primers to determine whether RBBP7/LSD1 binds to these genes. The PCR samples were separated and stained by electrophoresis in the 2% agarose gel containing ethidium bromide. The primers

for PCR are listed as the following: SOX2(5'->3'):F: GGCTTTGTTTGACTCCGTGT; R: TCCCATTGTCCCGACGTAAA. SOX9(5'->3'):F: AAAGCGGAGCTCGAAACTG; R: AAGTTTCCGGGGTTGAAACTG. OCT4(5'->3'):F: GCATTCCGTTGGCTATTC; R: GGGCAGCTCTAACCCTAAA. CCND1(5'->3'):F: CTCTGCCGGGCTTTGATCTT; R: ATGGTTTCCACTTCGCAGCA.

CRISPR/Cas9-mediated deletion of RBBP7-SE

The single-guide RNAs (sgRNAs) for deleting RBBP7-SE were designed by CRISPRscan (https://www.crisprscan.org) and CRISPRdirect (http://crispr.dbcls.jp). sgRNAs were annealed with NEBuffer2 in 95 °C 5 min, 70 °C 10 min. Annealed double-stranded DNA was inserted into the CRISPR/Cas9 PX458 vector using BbsI and BsaI (NEB, USA). Then the purified recombinant plasmid was transfected into the T-47D and MCF-7 cells in 24-well plates. The puromycin was added into cells after 48 h of transfection. After puromycin screening, cells were separated into 96-well plates by limiting dilution. PCR was amplified from the DNA isolated from homozygous (SE−/−) clones using external and internal primers of RBBP7-SE. The knockout plasmids of E1-E3 enhancer were transfected for 48 h and added with appropriate puro for 72 h, then the cells were collected to test the knockout efficiency and gene expression.

RNA extraction and qRT-PCR

Total RNA was extracted from cells using RNAiso Plus (TaKaRa, Dalian, China) according to the manufacturer's protocol, and then cDNA was synthesized by reverse transcription using PrimeScriptTM RT reagent Kit with gDNA Eraser (TaKaRa). qRT-PCR was performed by using FastStart Universal SYBR Green Master (Roche,

Basel, Switzerland) on an ABI 7500 Real-Time PCR System. Results were analyzed using the relative quantitative method and mRNA expression of genes was normalized with GAPDH. Primers of qRT-PCR were shown as the following: RBBP7(5'->3'):F: GTGGCCCAGTCTTACCGTTC; R: ATCAGACGTATGAGTCCCCAG. LSD1(5'->3'):F: GTGGACGAGTTGCCACATTTC; R: TGACCACAGCCATAGGATTCC. SOX2(5'->3'):F: TACAGCATGTCCTACTCGCAG; R: GAGGAAGAGGTAACCACAGGG. SOX9(5'->3'):F: TGGAAACTTCAGTGGCGCGGA; R: AGAGCAAAAGTGGGGGCGCTT. OCT4(5'->3'):F: CTTGAATCCCGAATGGAAAGGGR: GTGTATATCCCAGGGTGATCCTC. CCND1(5'->3'):F: GCTGCGAAGTGGAAACCATC; R: CCTCCTTCTGCACACATTTGAA.

Western blotting assays

For western blotting analysis, the total protein was extracted after lysis of cells with CelLytic buffer (Sigma-Aldrich, #C3228). The protein extracts were then loaded into SDS-PAGE with an SDS loading buffer. The protein was then transferred into a polyvinylidene fluoride (PVDF) membrane after separation. The membranes were then immersed in 5% milk for blocking of nonspecific binding for 1 h. The membranes were then incubated with primary and secondary antibodies. The overnight incubation of the primary antibody was followed by a 2-h incubation of the secondary antibody. The primary antibodies used in the present study were listed as the following: anti-RBBP7 (Abcam, ab259957), anti-E-cadherin (CST#3195), anti-N-cadherin (CST#13116), anti-Snail (CST#3879), anti-Vimentin (CST#5741), anti-H3K27ac (Abcam, ab4729), anti-SOX9 (Abcam, ab185966), anti-SOX2 (CST#23064), anti-OCT4 (CST#2750), anti-CCND1 (CST#55506), anti-β-actin (CST#4967).

Immunohistochemistry (IHC)

Paraffin-embedded BRCA tissue slides were baked at 60 °C for 2 h, deparaffinized in xylene, and rehydrated in alcohol. Endogenous peroxidase was blocked with 3% hydrogen peroxide for 10 min. Antigen retrieval was performed in citrate buffer, pH 6.0, in a steamer for 5 min. The slides were then blocked with 5% BSA for 1 h and incubated at 4 °C overnight with the indicated primary antibodies. The following day, the tissue sections were incubated with HRPconjugated secondary antibody for 1 h and detected using DAB substrates for 1 min followed by hematoxylin staining. The staining was evaluated by two pathologists blinded to the study results. The staining scoring criteria were as follows: staining intensity (negative = 0, weak = 1, moderate = 2, and strong = 3) and the extent of stained cells (0% = 0, 1–24% = 1, 25–49% = 2, 50–74% = 3 and 75–100% = 4).

In vitro limiting dilution tumorsphere formation assay

For the sphere formation assay, 2×10^3 BRCA cells were seeded into ultralow attachment 6-well plates. The cells were grown in serum-free DMEM/F-12 medium (Invitrogen) supplemented with 4 μg/ml insulin (Sigma-Aldrich), 20 ng/ml EGF (PeproTech), and 20 ng/ml basic FGF (Invitrogen). After incubation for 10 days, the sphere number was counted by microscopy. For in vitro limiting dilution assays, cells were plated in 96-well plates at 20, 40, 60, 80, or 100 cells per well, with eight replicates for each cell number. Ten days later, wells without spheres were counted. Limiting dilution analysis was performed using extreme limiting dilution analysis (http://bioinf.wehi.edu.au/software/elda/).

Organoid establishment assay

Organoids derived from human PDAC specimens were isolated and cultured as previously reported [23]. Briefly, fresh BRCA specimens were cut into small pieces and washed three times with cold PBS supplemented with

10% penicillin and streptomycin. Then, the tissues were digested with digestion buffer with 1% fetal bovine serum, 10% penicillin/streptomycin, 1.5 mg/mL collagenase type II, 500 U/mL type collagenase IV, 0.1 mg/mL dispase type II and 10 mM Y-27,632 (Selleck, Shanghai, China)) for 45 min at 37 °C with vigorous vibration. After digestion, the tumor pellets were washed with cold PBS three times and finally collected through centrifugation at 200×g for 5 min. Subsequently, tumor cells were embedded in Matrigel (BD) and plated in 96-well plates. After the polymerization of the Matrigel, these organoids were cultured in complete Advanced DMEM/F12 (Termo Fisher Scientific) supplemented with Noggin (0.1 mg/ml, PeproTech), R-spondin (1 μg/ml, Nuvelo), epidermal growth factor (EGF, 50 ng/ml, PeproTech), Glutamax (Invitrogen), HEPES (Invitrogen), N2 (Invitrogen), B27 (Invitrogen), N-acetyl-L-cysteine (1 mM, Sigma), gastrin (10 nM, Sigma), nicotinamide (10 mM, Sigma), A83-01 (0.5 mM, Tocris Bioscience) and fibroblast growth factor 10(FGF10, 100 ng/ml, PreproTech). The organoid medium was changed approximately every 3 days, and organoids were passaged approximately every 7 days according to their growth conditions.

Subcutaneous animal tumor model

Four-week old Balb/c male nude mice were obtained from Shanghai Lingchang Biotechnology Co., Ltd. (Shanghai, China). 2×10^6 treated BCa cells resuspended in 100 μl PBS were subcutaneously injected to the left flank of the mice, which were randomly divided into several groups ($N = 5$/Group). The tumor latency period is about 10 days. The observers and recorders in the study were blinded to the grouping. Tumor growth was monitored once a week using a caliper and tumor volumes were calculated by the following formula: Volume = 1/2 length×(width)^2.

In vivo tail vein injection model

A lung metastasis mouse model generated by tail vein injection of breast cancer cells was used to evaluate cell metastasis, and there were ten mice in each group. Briefly, 4×10^6 MDA-MB-231 or MCF-7 cells were injected into the tail vein of each nude mouse. After the mice were sacrificed, the lungs were paraffin-embedded, and routine HE staining was performed. Intrapulmonary metastases were observed with a Leica imaging system and photographed.

Statistical analysis

All experiments, except for those involving mice, were performed in at least three independent biological replicates, with technical replicates for each experiment. Data are expressed as the mean ± SD. For data with a normal distribution, unpaired or paired two-tailed Student's t-tests were used to compare the significance of differences between two groups of independent samples. For the in vivo experiments related to animals, the number of biological replicates is 4 or 5. Animals were allocated to control experimental groups using a blinding and randomization method. The survival rate was determined using the Kaplan–Meier method. Statistics were performed by GraphPad Prism 8.0. A *P*-value less than 0.05 was considered statistically significant.

Results

RBBP7 is overexpressed in BCa and correlates with poor clinical outcomes

To investigate the role of RBBP7 in tumorigenesis, we downloaded the expression data of RBBP7 in various cancer types from TCGA via the UCSC-Xena platform (https://xena.ucsc.edu/). Pan-cancer analysis revealed that RBBP7 was aberrantly up-regulated in multiple tumors, like lung adenocarcinoma (LUAD), colon cancer (COAD), uterine corpus endometrial carcinoma (UCEC), and head and neck squamous cell carcinoma (HNSCC) (Fig. 1A). Of note, RBBP7 levels were also relatively high in BCa compared to most other tumors (Fig. 1A). In line with the results derived from TCGA, we also analyzed that the expression of RBBP7 was elevated in BCa than normal tissues based on samples from GEO databases (Fig. 1B). In addition, 30 paired BCa and adjacent normal tissues were collected, and increased mRNA expression of RBBP7 was also detected in BCa samples via RT-qPCR (Fig. 1C). To confirm the statistical findings, we obtained resected samples from 8 human BCa patients and detected that RBBP7 proteins were significantly higher in tumor groups than normal (Fig. 1D). Furthermore, an immunohistochemistry (IHC) assay for tumor tissues and its corresponding normal tissues from 30 patients was performed, and we validated the same results (Fig. 1E). The Kaplan-Meier survival curves analysis implicated that high RBBP7 levels were associated with shorter recurrence free survival (RFS) and overall survival (OS) months, which were demonstrated in a series of GEO datasets (Fig. 1F). Collectively, these data concluded that RBBP7 is up-regulated in BCa and correlated with poor prognosis, suggesting that it may be an essential biomarker.

RBBP7 enhances BCa tumorigenicity and metastasis in vitro and in vivo

To determine the functional roles of RBBP7 in BCa, we screened the Cancer Cell Line Encyclopedia (CCLE) and compared the RBBP7 levels in a series of BCa cell lines. We therefore obtained the RBBP7^{high} (MCF-7, T-47D, ZR-75-1) and RBBP7^{low} (MDA-MB-231, MDA-MB-453, HS-578T) cell groups, which were further validated by RT-qPCR and western blotting assays (Fig. 2A). Then, we

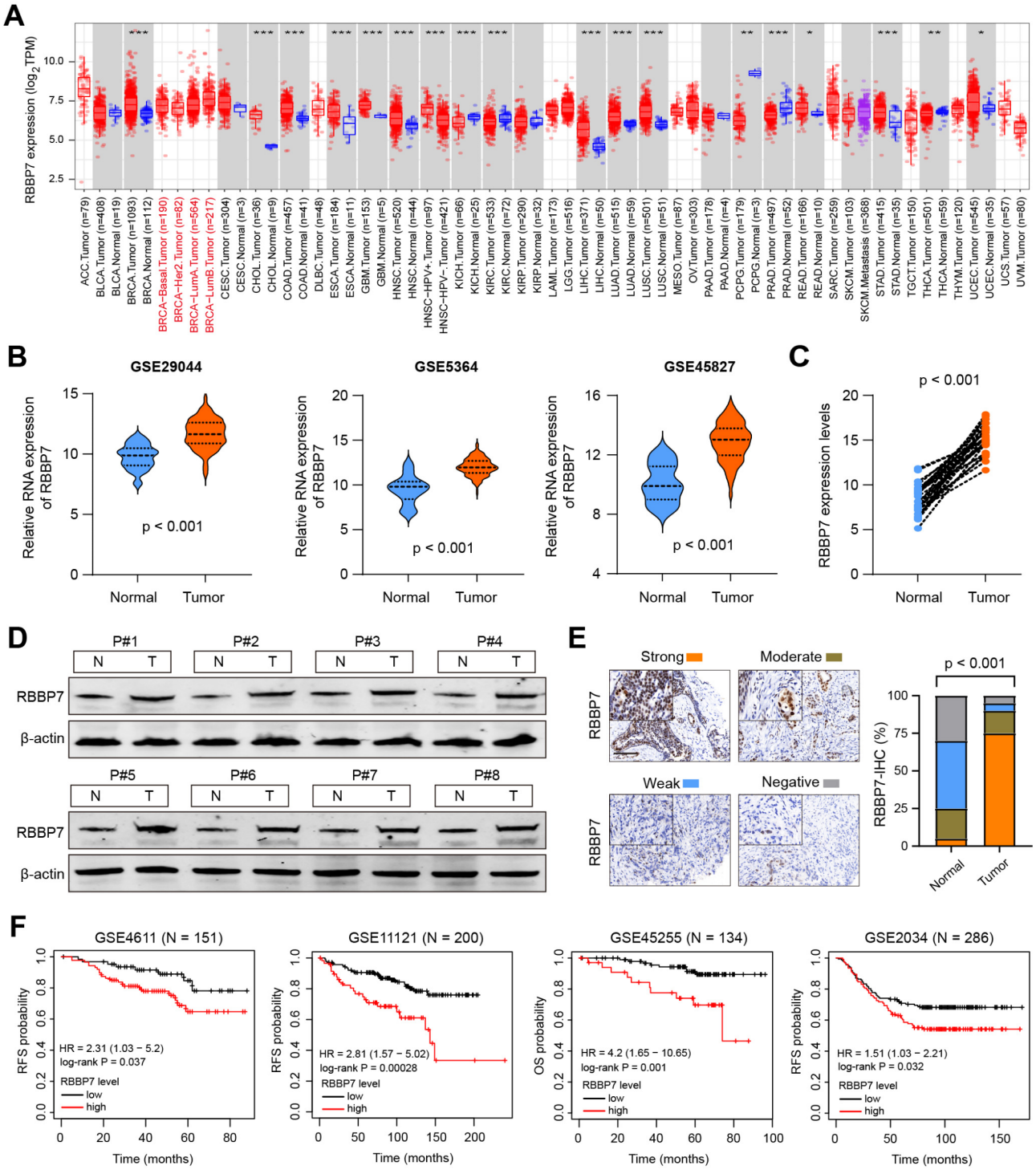

Fig. 1 Overexpression of RBBP7 in human BRCA was correlated with poor-disease outcome. **(A)** Pan-cancer analysis showing the RBBP7 expression levels across various tumors via TIMER. **(B)** Differential analysis of RBBP7 mRNA levels in BCa tumor samples and matched normal tissues was conducted in GSE29044 (left), GSE5364 (middle), and GSE45827 (right). **(C)** RT-qPCR analysis showing the expressions of RBBP7 in breast cancer tissues or normal control tissues. **(D)** Western blot analysis of RBBP7 proteins in 8 paired BCa tumor tissues (T) and adjacent nontumor tissues (N). **(E)** RBBP7 expressions were detected and categorized by IHC. Scale bar = 50 μm. **(F)** BCa patients were divided into two subsets with low and high RBBP7 levels. Kaplan-Meier analysis was used to compare the differential outcomes between RBBP7-high and -low patients that were obtained from publicly GEO datasets. Data represent the Mean ± SD of at least three independent experiments. *$P < 0.05$, **$P < 0.01$, and ***$P < 0.001$. Differences were tested using a un-paired Student's t-test **(B, C)**, and the log-rank test **(F)**

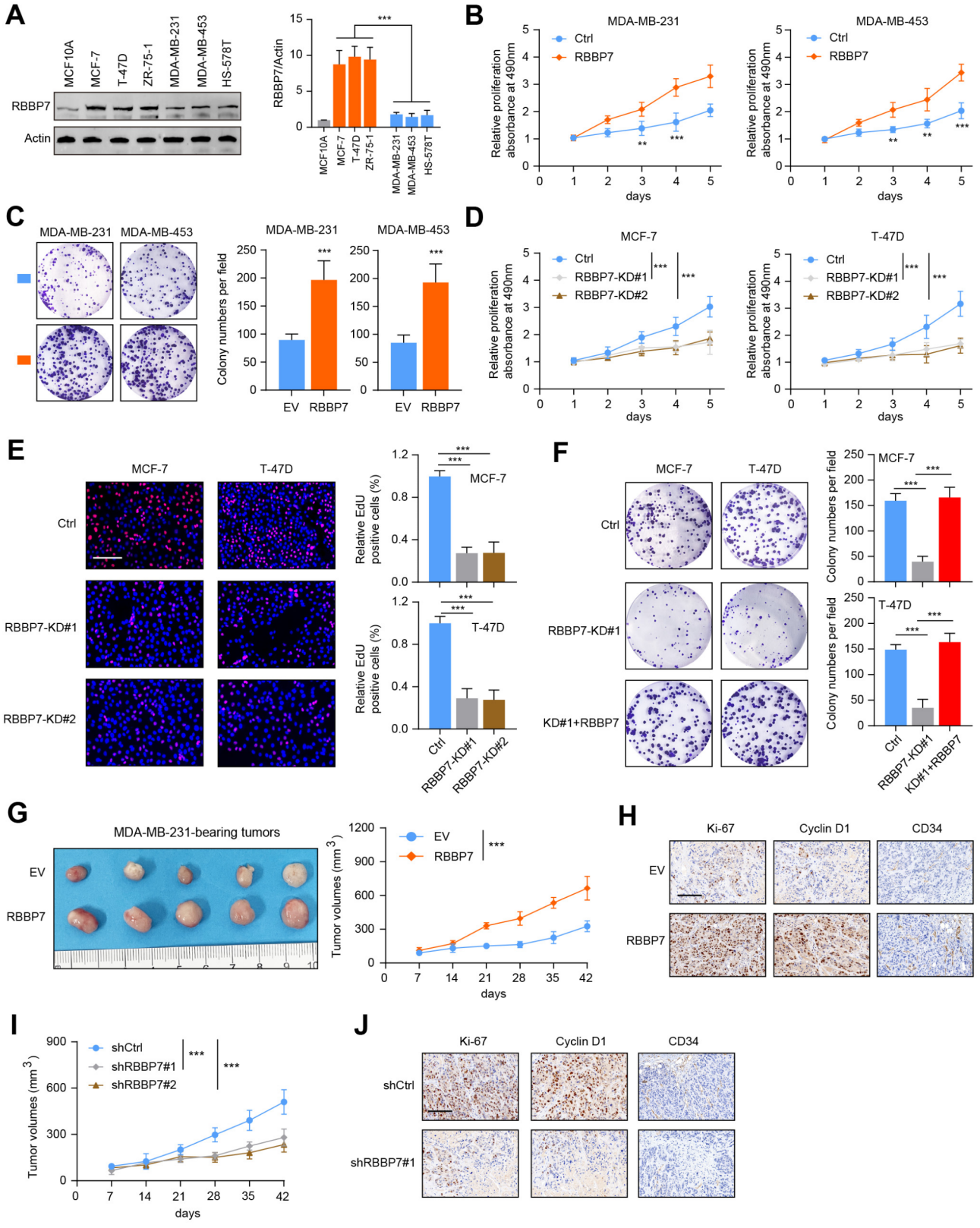

Fig. 2 (See legend on next page.)

(See figure on previous page.)

Fig. 2 RBBP7 enhanced BCa cell growth in vitro and in vivo. **(A)** The protein and mRNA levels of RBBP7 in normal breast epithelial cell MCF-10 A and breast cancer cell lines was detected and compared by western blot or qRT-PCR. **(B)** Cell proliferation was detected and compared by CCK-8 assay at the indicated time points in Ctrl and RBBP7-overexpressing (MDA-MB-231, MDA-MB-453) cells. **(C)** Colony formation assays were conducted in Ctrl and RBBP7-overexpressing (MDA-MB-231, MDA-MB-453) cells. **(D)** Cell proliferation was detected and compared by CCK-8 assay at the indicated time points in Ctrl and RBBP7-KD (MCF-7, T-47D) cells. **(E)** The EdU assays were conducted to assess the effect of RBBP7 overexpression on cell proliferative ability. Scale bar = 100 μm. Quantitative data was shown on the right. **(F)** Cell growth was assessed by colony formation assay. The rescue assays were performed by ectopic expression of RBBP7. **(G)** Representative BCa tumor images per group at the experimental ending were shown (left) and tumor growth curve was generated (right). **(H)** IHC assays showing the expression levels of Ki-67, CCND1, and CD34 in tumors derived from Ctrl and RBBP7-overexpressing cells. **(I)** Tumor growth curve was generated and compared between shCtrl and shRBBP7 groups. **(J)** IHC assays showing the expression levels of Ki-67, CCND1, and CD34 in tumors derived from Ctrl and RBBP7-KD cells. Data represent the Mean ± SD of at least three independent experiments. $^{*}P < 0.05$, $^{**}P < 0.01$, and $^{***}P < 0.001$. Differences were tested using the 2-way ANOVA followed by Tukey's multiple comparisons test **(B**, **D**, **G**, **I)**

generated stable RBBP7-overexpressing (MDA-MB-231, MDA-MB-453) and RBBP7 knockdown (MCF-7, T-47D, ZR-75-1) BCa cells. The transfection efficiency in each indicated cell line was examined by western blotting (Figure S1A-B). Then, we found that RBBP7 overexpression markedly enhanced BCa cell proliferation, as evidenced by MTT and colony formation assays (Fig. 2B-C). The EdU incorporation assay further confirmed that RBBP7 could induce increased DNA synthesis (Figure S1C). In contrast, RBBP7 knockdown significantly led to decreased cell proliferation, and DNA synthesis activities (Fig. 2D-E). Although RBBP7 deficiency abrogated the colony formation abilities, ectopic overexpression of RBBP7 rescued the impaired phenotype and enhanced cell growth (Fig. 2F). To further explore whether RBBP7 modulates BCa growth in vivo, we carried out the tumor xenograft experiments using RBBP7-overexpressing MDA-MB-231 cells. Xenograft tumor models suggested that RBBP7 overexpression notably enhanced tumor growth, as indicated by representative tumor graphs or tumor volume curves (Fig. 2G and Figure S1D). Consistent with the results, immunostaining assays exhibited elevated levels of Ki-67 (a biomarker of proliferation) and CD34 (a biomarker of angiogenesis), in the tumors derived from the RBBP7-overexpressing group compared with those in control (Fig. 2H). In contrast, the knockdown of RBBP7 remarkably inhibited tumor growth, showing a markedly smaller tumor size and decreased levels of oncogenic markers (Fig. 2I-J and Figure S1E). Therefore, these results suggested that RBBP7 is required for tumor growth in vitro and in vivo.

We further discovered the functional role of RBBP7 in driving the metastasis phenotypes of BCa cells in vitro or in vivo. Therefore, transwell and scratch wound healing assays were performed to determine cell migration or invasion properties. As indicated in Figure S1F, RBBP7 deficiency prominently inhibited the invasion and migration capacities of MCF-7 and T-47D cells. Conversely, RBBP7 overexpression potentiated the above abilities of MDA-MB-231 and MDA-MB-453 cells (Figure S1G). As documented, Epithelial-mesenchymal transition (EMT) is an essential process, by which epithelial cells are transcriptionally reprogrammed to obtain decreased adhesion and increased migration abilities. We thus detected typical EMT markers (E-cadherin, N-cadherin, Snail1, and Vimentin) via western blotting in different cell groups. We observed that RBBP7 overexpression enhanced a mesenchymal phenotype in MDA-MB-231, or MDA-MB-453 cells, as shown by the downregulation of E-cadherin and upregulation of N-cadherin, Vimentin, and Snail1 (Fig. 3A). We proposed that RBBP7 participates in the EMT process to potentiate the migration or invasion abilities of BCa cells. To further assess the impact of RBBP7 on BCa in vivo metastasis, we constructed stable RBBP7-overexpressing MDA-MB-231-luciferase cells and control cells, which were injected into the tail vein of BALB/c nude mice. The luciferase signals of metastases in the lung were detected and compared at regular time points. After 5 weeks, RBBP7 overexpression remarkably enhanced BCa lung metastasis, as evidenced by bioluminescence graphs and lung metastatic nodes (Fig. 3B-C). H&E-stained lung sections also proved that mice in the RBBP7-overexpressing group suffered from more metastatic burden than those in the control group (Fig. 3D). In contrast, MCF-7 cells with RBBP7 ablation markedly inhibited BCa lung metastasis, as evidenced by the luciferase signal and number of lung metastatic lesions compared with those from the control group (Fig. 3E-F). Collectively, these data support the important role of RBBP7 in driving BCa metastasis.

RBBP7 is a novel SE-driven oncogene in BCa

To explore detailed mechanisms that drive high RBBP7 expressions in BCa, we queried the Cistrome Data Browser (http://cistrome.org/db/#/) to seek transcription al regulation or modifications on the RBBP7 promoters or enhancers. Through the analysis of H3K27ac peaks from the Cistrome dataset, we observed the H3K27ac enrichment level of the super-enhancer in BCa cells (Fig. 4A). The SE regions were mainly classified by the ranking method based on the H3K27ac signal (ROSE). Interestingly, we also found this super-enhancer in another kind of tumor cells, like A549, HeLa, and HCT-116 (Fig. 4A). However, this super-enhancer was nearly undetectable in normal cell lines, like MCF-10 A (Fig. 4A). Apart from H3K27ac, we also found other SE-related features

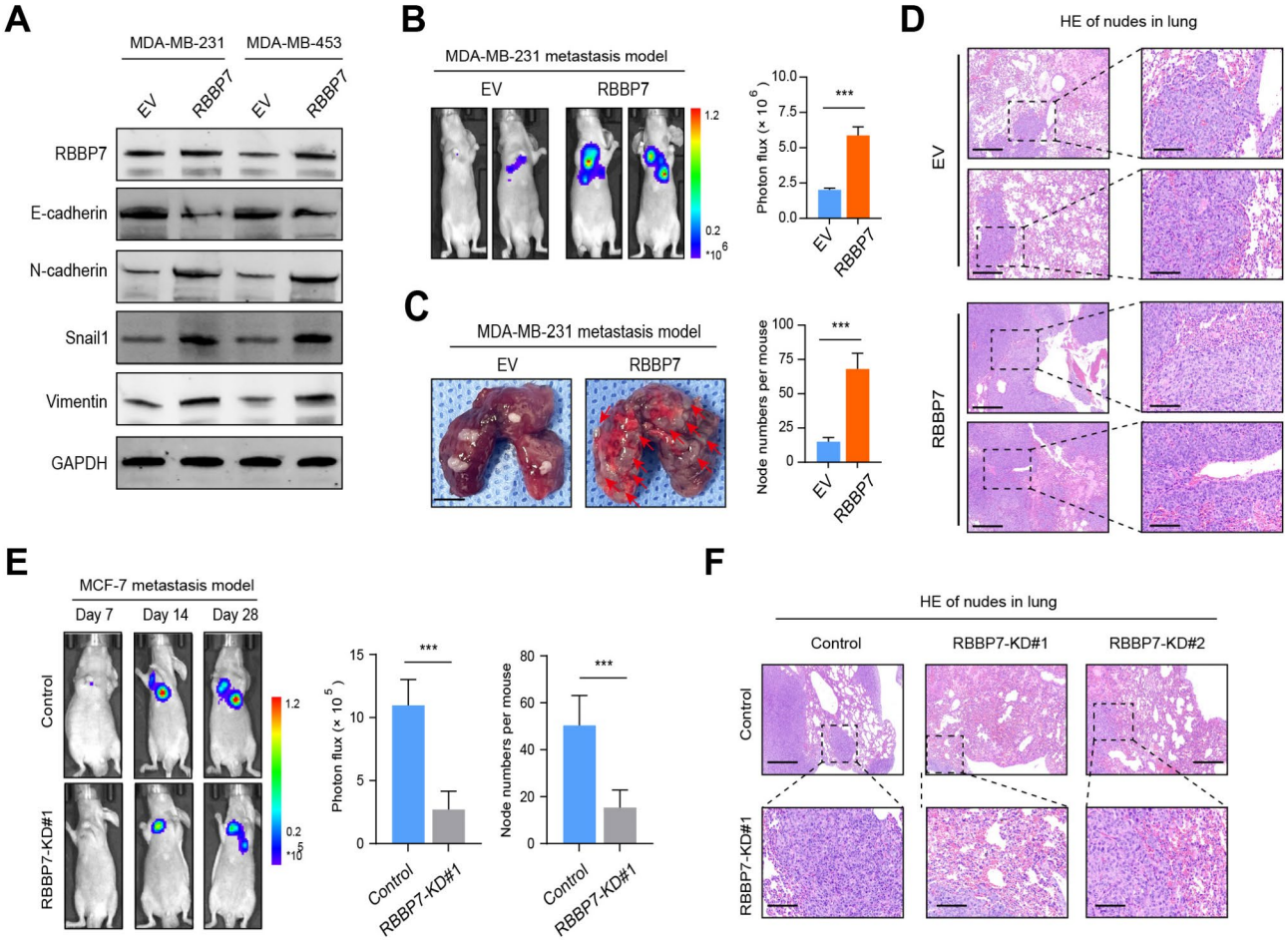

Fig. 3 RBBP7 potentiates EMT and tumor stemness in BCa in vitro and in vivo. **(A)** Relationships between RBBP7 and EMT markers were shown by western blotting assays in MDA-MB-231 and MDA-MB-453 cells. **(B)** Representative BLI images for control and RBBP7-overexpressing MDA-MB-231 cells at indicated timepoints. Lung metastasis is calculated as the mean ± SEM of the bioluminescence signal at day 28. **(C)** Representative lung images of distal metastasis are shown on the left, and the numbers of metastases are quantified on the right. **(D)** HE graphs showing lung metastases in mice derived from EV and RBBP7 groups. Scale bar, 200 μm (left); Scale bar, 50 μm (right). **(E)** Representative BLI images for control and RBBP7-KD MCF-7 cells at indicated timepoints. Lung metastasis is calculated (right) as the mean ± SEM of the bioluminescence signal at day 28. **(F)** HE graphs showing lung metastases in mice derived from Control and RBBP7-KD groups. Scale bar, 200 μm (left); Scale bar, 50 μm (right). Data represent the Mean ± SD of at least three independent experiments. $^{*}P < 0.05$, $^{**}P < 0.01$, and $^{***}P < 0.001$. Differences were tested using a un-paired Student's t-test **(A-D, F-G, I)**

within this region, like p300, and DNase I hypersensitivity (Fig. 4A). We further divided this super-enhancer into three indicated regions, including E1-3, and ChIP-qPCR analysis confirmed the active histone modifications on the above enhancer regions in BCa cells (Fig. 4B). Then, we utilized the CRIPSR-Cas9 technology to delete the region of RBBP7-SE bound by p300, and obtained the $SE^{-/-}$ MCF-7 and $SE^{-/-}$ T-47D cell clones (Fig. 4C-D). RT-qPCR analysis revealed that RBBP7 levels were notably suppressed in SE-deleted cells compared to that of the control wild-type in MCF-7 or T-47D cells (Fig. 4E). Besides, we also designed two specific siRNAs targeting p300, and p300 knockdown effectively reduced the mRNA or protein levels of RBBP7 (Fig. 4F). Several small-molecule BET inhibitors (BETi), like JQ1 or THZ1, have shown profound efficacy in abrogating SE structure and suppress SE-driven tumors. We thus treated MCF-7 and T-47D cells with JQ1 and confirmed that JQ1 could substantially decrease RBBP7 expressions in a dose-dependent manner (Fig. 4G).

Last of all, we validated the functional role of RBBP7-SE on BCa malignant features. CCK-8 assays revealed that RBBP7-SE deletion significantly inhibited cell growth rates (Fig. 4H-I). Besides, we overexpressed RBBP7 in $SE^{-/-}$ MCF-7 and $SE^{-/-}$ T-47D cells, respectively (Fig. 4J). As expected, $SE^{-/-}$ MCF-7 and $SE^{-/-}$ T-47D cells revealed impaired colony formation efficiency and slower migratory speed relative to parental cells, which could be completely rescued by RBBP7 overexpression (Fig. 4K). Collectively, these findings indicate that RBBP7-SE governs RBBP7 expressions to drive BCa growth and migration.

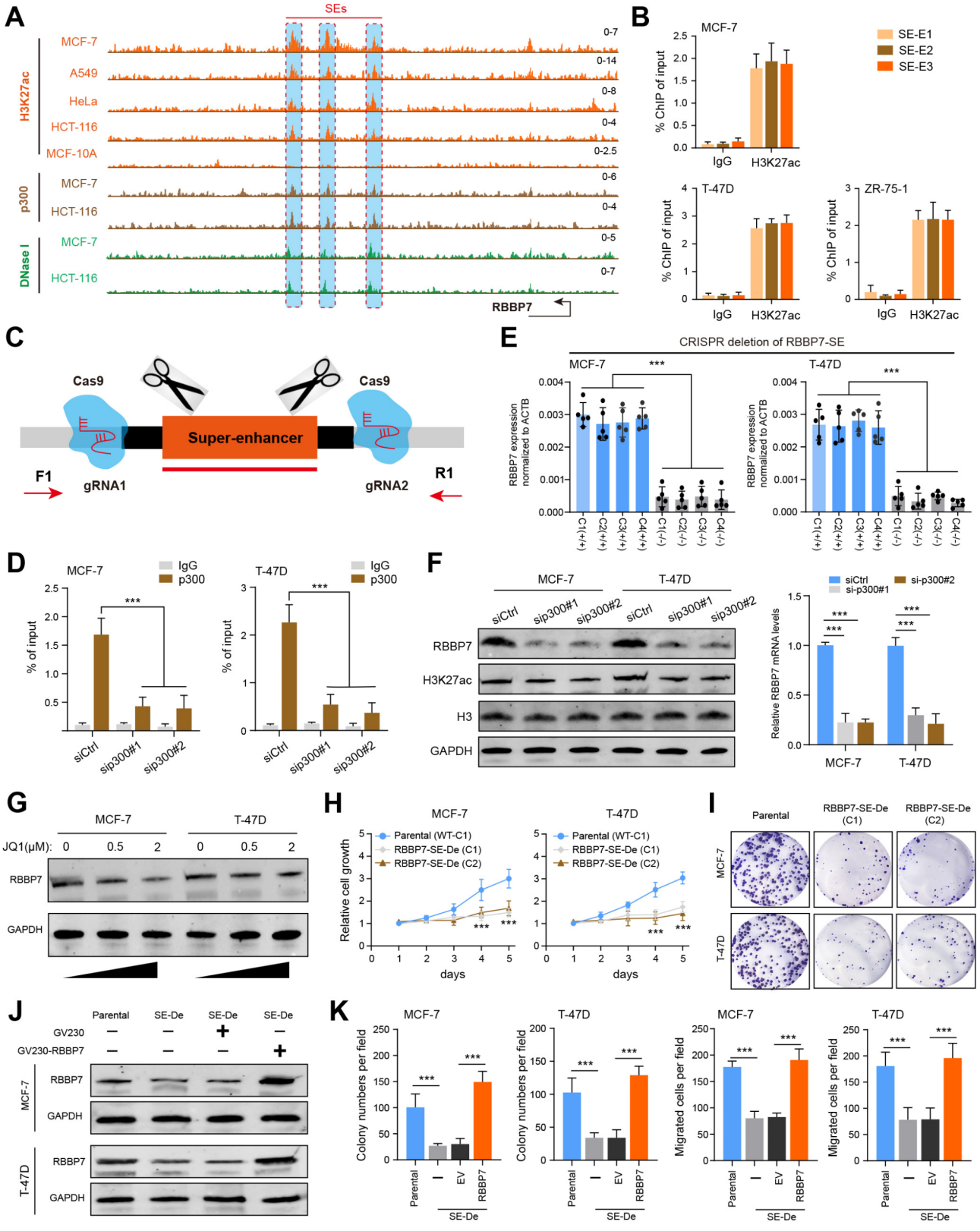

Fig. 4 (See legend on next page.)

(See figure on previous page.)

Fig. 4 Identification of a super-enhancer that drives RBBP7 expressions in BCa. **(A)** The putative enhancers of the super-enhancer (E1-E3) were identified based on markers of H3K27ac, P300, and DNase I in HeLa, HCT-116 and MCF-7 cells. **(B)** ChIP-qPCR analysis showing the H3K27ac enrichment on RBBP7-SEs in MCF-7, T-47D, and ZR-75-1 cells. **(C)** Illustration of genetic deletion of RBBP7-SE regions via CRISPR sgRNA technology. **(D)** ChIP-qPCR analysis showing the p300 enrichment on RBBP7-SE in Ctrl and p300-KD MCF-7 or T-47D cells. **(E)** ChIP-qPCR analysis of RBBP7 mRNA expression in 4 WT cell clones and 4 clones with CRISPR-deleted RBBP7-SE ($n=5$). **(F)** Western blot and RT-qPCR analysis comparing the expression levels of RBBP7 in control and p300-KD cells (MCF-7, T-47D). **(G)** Western blot showing the RBBP7 expressions in response to increasing doses of JQ1 treatment. **(H)** CCK-8 analysis showing the cell proliferation rates of BCa cells (MCF-7, T-47D) with or without RBBP7-SE depletion. **(I)** Colony formation assays showing the growth capacities of BCa cells (MCF-7, T-47D) with or without RBBP7-SE depletion. **(J)** Western blotting assays showing the RBBP7 levels in MCF-7, and T-47D cells. The overexpression vector GV230-RBBP7 was constructed to express RBBP7-EGFP fusion protein, and then transfected into the RBBP7-SE homozygous deletion $SE^{-/-}$ cell lines. **(K)** Proliferation and migration abilities were measured by colony formation and transwell assays. Data represent the Mean ± SD of at least three independent experiments. $^{*}P<0.05$, $^{**}P<0.01$, and $^{***}P<0.001$. Differences were tested using a un-paired Student's t-test (B, D, E, F, K) and the 2-way ANOVA followed by Tukey's multiple comparisons test **(H)**

RBBP7 potentiates stem-like properties of BCSCs via inducing stemness-related signature

To thoroughly figure out how RBBP7 regulates BCa development, we intended to calculate the potential downstream pathways related to RBBP7 via bioinformatic analysis. First, we obtained the expression data of RBBP7 from 1097 individuals diagnosed with invasive breast carcinoma and thus categorized them into high-, middle-, and low groups (Fig. 5A). Differential genes between RBBP7-high and -low groups were identified and GO analysis revealed several RBBP7-related biological items, including cell cycle, mTOR, and Hippo signaling (Fig. 5B). Besides, Gene Set Enrichment Analysis (GSEA) also demonstrated that high expression of RBBP7 was positively associated with the self-renewal pathway (Fig. 5C), indicating that RBBP7 might modulate the stemness process during BCa development. As shown in Fig. 5D, ectopic expression of RBBP7 increased the sphere formation capacities of BCa cells. However, RBBP7 knockdown suppressed the sphere formation abilities of CSCs compared with those in control cells (Fig. 5E). In addition, we also conducted the in vitro limiting dilution assays to quantitatively assess the effect of RBBP7 on breast cancer stem cell (BCSC) frequency. We found that RBBP7 overexpression efficiently increased breast CSC frequency in MDA-MB-231, MDA-MB-453, and HS-578T cells (Fig. 5F), whereas RBBP7 knockdown dramatically decreased the CSC frequency in MCF-7 and T-47D cells (Fig. 5G).

Next, we detected the stemness-related genes in RBBP7-overexpressing cells and found SOX2/SOX9/OCT4/CCND1 were all positively regulated by RBBP7 (Fig. 5H-I). Targeting RBBP7 also inhibited the expression levels of these genes in MDA-MB-231 and MDA-MB-453 cells, as implicated by RT-qPCR and western blotting assays (Fig. 5H-I). ChIP-qPCR analysis confirmed that RBBP7 could directly bind to the promoters of these genes, whereas RBBP7 knockdown abolished the binding connections (Fig. 5J-K). Luciferase assays also indicated that RBBP7 could induce trans-activation of the promoters of the four genes (Figure S2A). Conversely, RBBP7 inhibition substantially abrogated the promoter activity of the above genes (Figure S2B). Considering RBBP7-SE activates RBBP7 expressions, we found that RBBP7-SE-deleted MCF-7 or T-47D cells showed decreased SOX2/SOX9/OCT4/CCND1 levels and impaired stemness capacities (Fig. 5L-M). Taken together, our results clarified that RBBP7 sustained BCa stemness via trans-activating stemness-related genes.

RBBP7 recruits demethylase LSD1 to trans-activate stemness genes via epigenetic remodeling

In addition, we also wondered about the molecular mechanisms by which RBBP7 maintains high expressions of downstream stemness genes. Given that RBBP7 belongs to a subunit of the NuRD complex, we thus intended to explore whether other NuRD subunits may contribute to the epigenetic functions of RBBP7. First, we performed an immunoprecipitation (IP) assay to screen and characterize RBBP7-associated NuRD factors. As indicated, MCF-7 cells were transfected with FLAG-RBBP7, and the subsequent IP was performed via an anti-FLAG antibody. As expected, RBBP7 associated with several NuRD complex components, like HDAC1, MAT1/2, CHD4, MBD2, and LSD1 (Fig. 6A). However, knocking down LSD1 but not other subunits could efficently inhibit BCa renewal abilities and induce down-regulated expressions of CSC signature genes (Fig. 6B-C and Figure S2C). ChIP-qPCR assays confirmed that LSD1 is directly bound to the promoters of RBBP7-regulating stemness genes. As reported, phosphorylation of the C-terminal domain (CTD) of RNA polymerase II (Pol II) is an essential prerequisite for transcription initiation. Interestingly, ChIP-qPCR analysis on the above promoter regions implicated that both Ser5- and Ser2-phosphorylated RNA Pol II CTDs were decreased when LSD1 was depleted (Fig. 6D). Consistently, LSD1-mediated H3K9me3 demethylation contributes to activate genes transcription, and targeting LSD1 significantly increased suppressive H3K9me3 enrichment on the promoters of SOX2/SOX9/OCT4/CCND1 (Fig. 6E). However, RBBP7 deficiency prevented the recruitment of LSD1 to the promoter regions of SOX2/SOX9/OCT4/CCND1 and further decreased levels of Ser5- and Ser2-phosphorylated RNA Pol II CTDs

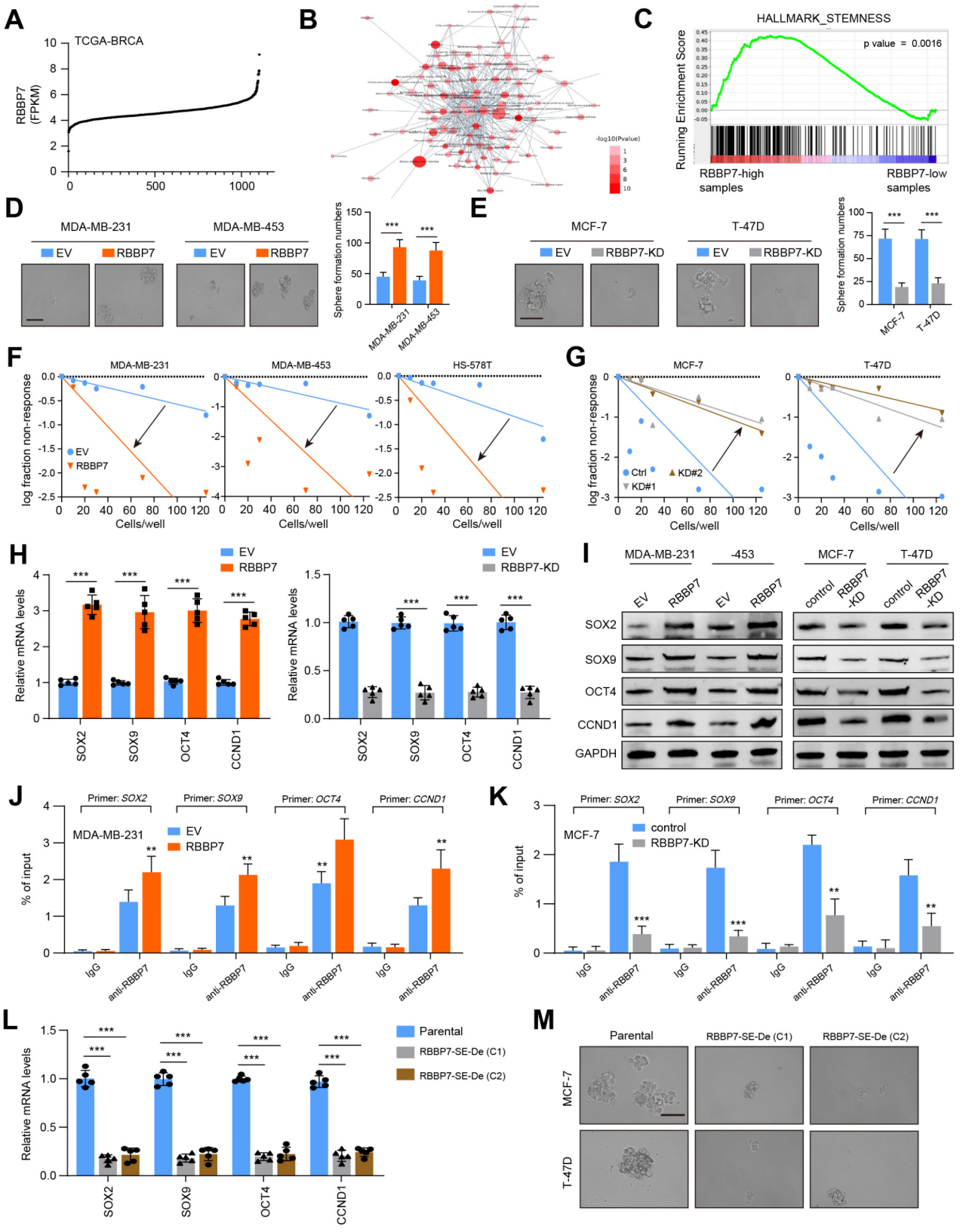

Fig. 5 (See legend on next page.)

(See figure on previous page.)

Fig. 5 RBBP7 promotes BCa stemness features. **(A)** Overall distribution of RBBP7 expression data in patients from TCGA-BCa cohort. **(B)** Gene Ontology (GO) analysis based on RBBP7-related DEGs. **(C)** Gene Set Enrichment Analysis (GSEA) was conducted between RBBP7-high and RBBP7-low samples. **(D)** Representative images and quantification of the in vitro sphere-formation assay of RBBP7-overexpressing BCa (MDA-MB-231, MDA-MB-453) cells and control cells ($n=6$). Scale bar = 200 μm. **(E)** Representative images and quantification of the in vitro sphere-formation assay of RBBP7-KD BCa (MCF-7, T-47D) cells and control cells ($n=6$). Scale bar = 200 μm. **(F)** In vitro limiting dilution assay of RBBP7-OE and control BCa cells. A well not containing spheres (diameter ≥ 50 μm) was defined as a non-response. **(G)** In vitro limiting dilution assay of RBBP7-KD and control BCa cells. **(H)** RT-qPCR analysis showing the mRNA levels of SOX9/SOX2/OCT4/CCND1 in RBBP7-OE (left) or RBBP7-KD (right) cells. **(I)** Western blot assays showing the protein levels of SOX9/SOX2/OCT4/CCND1 in RBBP7-OE (left) or RBBP7-KD (right) cells. **(J)** ChIP-qPCR analysis showing the RBBP7 enrichment on the indicated promoter regions of SOX9/SOX2/OCT4/CCND1 in control or RBBP7-OE MDA-MB-231 cells. **(K)** ChIP-qPCR analysis indicated the impaired RBBP7 enrichment on the indicated promoter regions of SOX9/SOX2/OCT4/CCND1 in control or RBBP7-KD MCF-7 cells. **(L)** RT-qPCR analysis showing the mRNA levels of SOX9/SOX2/OCT4/CCND1 in parental control or RBBP7-SE-deleted MCF-7 cells. **(M)** Representative graphs showing the in vitro sphere-formation assay of RBBP7-SE-deleted BCa (MCF-7, T-47D) cells and control cells ($n=6$). Scale bar = 200 μm. Data represent the Mean ± SD of at least three independent experiments. $^{*}P<0.05$, $^{**}P<0.01$, and $^{***}P<0.001$. Differences were tested using a un-paired Student's t-test **(D**, **E**, **H**, **J**, **K**, **L)**

(Fig. 6F and Figure S2D). However, LSD1 overexpression failed to effectively restore levels of Ser5- and Ser2-phosphorylated RNA Pol II CTDs in RBBP7-deficient cells, indicating that RBBP7 is an essential intermediate for LSD1 recruitment to promoters (Fig. 6G). RT-qPCR assays further demonstrated that RBBP7 relied on LSD1 to elevate stemness signature genes in MDA-MB-231 or MDA-MB-453 cells (Fig. 6H). In line with the findings, the knockdown of LSD1 dramatically inhibited colony formation, cell migration, and invasion abilities (Figure S2E-G). In addition, LSD1 knockdown could markedly impair RBBP7-induced BCa growth and angiogenesis in vivo (Fig. 6I-K). Thus, our data supported that RBBP7 maintains self-renewal capacities and promotes BCa malignant progression through the recruitment of LSD1.

LSD1 specific inhibitor (ORY-1001) effectively inhibits tumor stemness, proliferation, and metastasis for RBBP7high BCa

Given the potential roles of LSD1 in facilitating RBBP7^{high} BCa progression, we intended to introduce ORY-1001, a specific LSD1 inhibitor that targets lysine-specific demethylase. Based on the previously categorized normal or BCa cell lines, we observed that RBBP7^{high} BCa cells were preferentially sensitive to ORY-1001 (IC_{50} between 10 and 20 nM), whereas normal and RBBP7^{low} BCa cells were resistant (IC_{50} > 1000 nM) to ORY-1001 (Fig. 7A). Concordantly, ORY-1001 inhibited the growth of MCF-7 and T-47D cells in a dose-dependent manner (Fig. 7B). Although RBBP7 overexpression potentiated BCa stemness capacities, ORY-1001 administration markedly abrogated the RBBP7-induced effects (Fig. 7C). RT-qPCR analysis also proved that ORY-1001 could inhibit the mRNA expressions of SOX2/SOX9/OCT4/CCND1 (Fig. 7D). To validate the clinical significance of ORY-1001, patient-derived BCa samples were obtained to generate patient-derived-organoids (PDOs) or -xenografts (PDXs) for translational research (Fig. 7E). We performed an organoid assay on RBBP7^{high} and RBBP7^{low} samples with or without ORY-1001 administration. As expected, ORY-1001 markedly suppressed the growth of RBBP7^{high} organoids, with an imperceptible effect in RBBP7^{low} organoids (Fig. 7F).

We further pharmacologically characterized a specific LSD1 inhibitor, ORY-1001, in animal BCa models. First, we treated mice with either ORY-1001 (0.02 mg/kg) or a DMSO vehicle once daily for 7 weeks. The ORY-1001 treatment with daily oral gavage did not induce any unhealthy side effects in mice, which have normal body weight and blood counts (Figure S3A-B). The safety of ORY-1001 was also validated by the H&E staining analysis in different organs of mice (Figure S3C). Then, we adopted patient-derived xenografts (PDXs) exhibiting high or low RBBP7 levels (Fig. 7G). Quantified by the tumor volumes, ORY-1001 treatment was more efficient at limiting RBBP7-high PDX tumors than RBBP7-low tumors (Fig. 7H). IHC analysis revealed that ORY-1001 could notably suppress stemness and angiogenesis in RBBP7-high tumors, along with decreased SOX2/OCT4/CCND1/CD31 levels (Fig. 7I). Last of all, we determined the efficacy of ORY-1001 in suppressing BCa distant metastasis. The tail vein injection models implicated that ORY-1001 can notably suppress the metastatic capacities of MCF-7 cells, but exerted limited effects in models derived from MDA-MB-231 cells (Fig. 7J), as assessed by the metastatic numbers in the lung (Fig. 7K). Collectively, these findings concluded that ORY-1001 could efficiently suppress the progression of RBBP7^{high} BCa, but not the RBBP7^{low} subtypes (See Fig. 8).

Discussion

Served as essential members involved in histone metabolism, histone chaperones facilitate histone binding to DNA and promote nucleosome formation [24]. RBBP4/7 both belong to histone chaperones and modulate gene expressions via the interactions of their WD40 domain with the histone H4 and H3 [25]. Abnormal chromatin remodeling process induced by RBBP4/7 may lead to altered gene expression levels, thereby contributing to tumorigenesis and other diseases. Multiple researches have implicated that RBBP7 is highly expressed in hepatocellular carcinoma, colon cancer, and esophagus cancer [10, 26]. Here, we also found that RBBP7 was highly

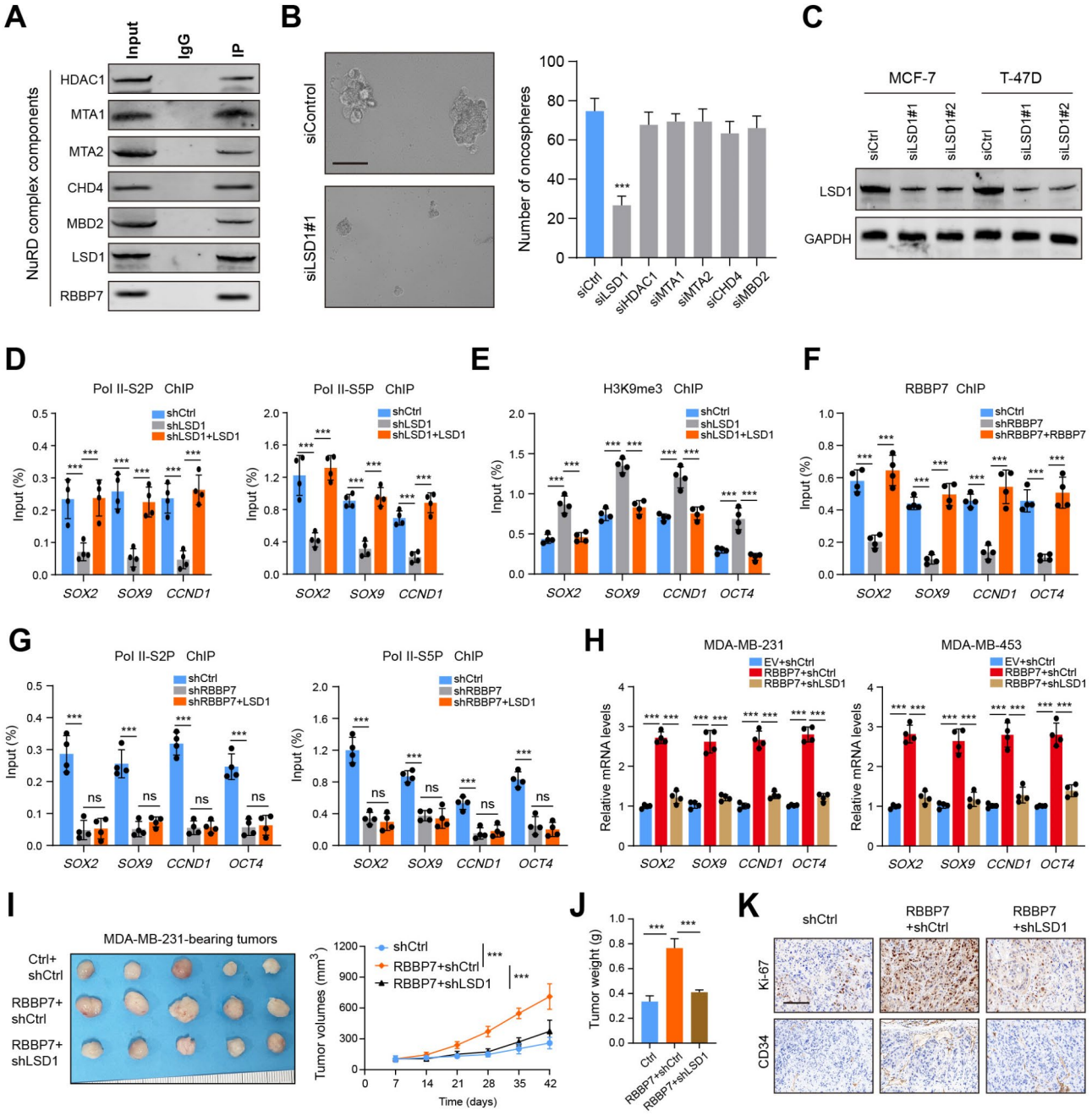

Fig. 6 RBBP7 recruits demethylase LSD1 to epigenetically regulate SOX9/SOX2/OCT4/CCND1 levels. **(A)** Co-IP and western blot assays showing the potential interactions between RBBP7 and a series of NuRD complex components. **(B)** Representative graphs showing the in vitro sphere-formation assay that were conducted in control and siRNA-treated MCF-7 cells. **(C)** Western blot assays showing the knocking down RBBP7 expressions in cells treated with or without siRNA. **(D)** ChIP-qPCR analysis of Pol II-S2P (left) and S5P (right) in the promoter regions of the indicated targets in WT and LSD1-KD MCF7 cells with or without LSD1 restoration. **(E)** ChIP-qPCR analysis of H3K9me3 enrichment on the promoters of genes in WT and LSD1-KD MCF7 cells with or without LSD1 restoration. **(F)** ChIP-qPCR analysis of RBBP7 enrichment on the promoters of genes in WT and RBBP7-KD MCF7 cells with or without RBBP7 restoration. **(G)** ChIP-qPCR analysis of Pol II-S2P (left) and S5P (right) in the promoter regions of the indicated targets in control and RBBP7-KD MCF7 cells with or without LSD1 restoration. **(H)** RT-qPCR analysis revealing the mRNA levels of SOX9/SOX2/OCT4/CCND1 in RBBP7-overexpressing MDA-MB-231 or MDA-MB-453 cells with or without LSD1 knockdown. **(I)** Graphs and tumor volumes of indicated MDA-MB-231-cell-derived xenograft tumors (Ctrl-shCtrl group, RBBP7-shCtrl group, and RBBP7-shLSD1 group). **(J)** Quantification of tumor weight in tumors derived from indicated groups in **(I)**. **(K)** IHC graphs of Ki-67, and CCND1 markers in tumors derived from indicated groups in (**I**). Data represent the Mean ± SD of at least three independent experiments. **P* < 0.05, ***P* < 0.01, and ****P* < 0.001. Differences were tested using a un-paired Student's t-test **(B, D-H, J)**, and the 2-way ANOVA followed by Tukey's multiple comparisons test **(I)**

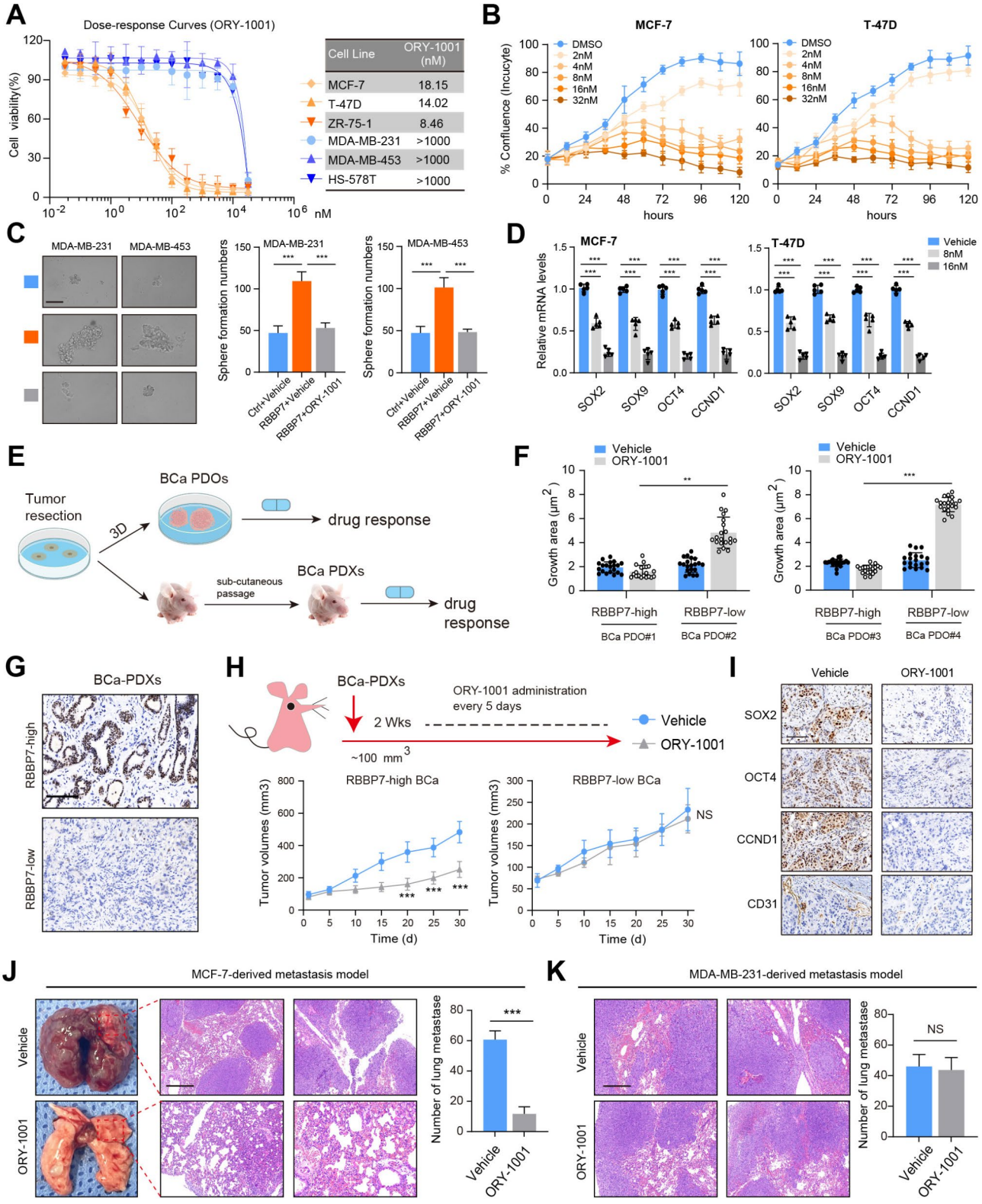

Fig. 7 (See legend on next page.)

(See figure on previous page.)

Fig. 7 LSD1 specific inhibitor (ORY-1001) is effective to suppress RBBP7^{high} BCa. **(A)** Dose-response curves and IC50 data in a list of BCa (RBBP7-high, and RBBP7-low) cells treated with ORY-1001. **(B)** CCK-8 assays revealed the cell viability of RBBP7-high BCa cells treated with increasing doses of ORY-1001. **(C)** Representative images of tumor sphere formation and quantification of spheres in RBBP7-overexpressing MDA-MB-231 or MDA-MB-453 cells with or without ORY-1001 treatment. **(D)** RT-qPCR analysis detecting the mRNA levels of SOX9/SOX2/OCT4/CCND1 in MCF-7 or T-47D cells treated with increasing doses of ORY-1001. **(E)** Flowchart showing the generation of BCa patients-derived organoids (PDOs) and xenografts (PDXs). **(F)** Quantification of RBBP7-high and RBBP7-low BCa organoids with or without ORY-1001 treatment. **(G)** Representative IHC images of RBBP7 staining levels in tumors from RBBP7-high or RBBP7-low PDXs. **(H)** Tumor volumes of indicated RBBP7-high, or RBBP7-low BCa PDXs treated with ORY-1001. **(I)** Representative IHC images of SOX2/CCND1/OCT4/CD31 in tumors derived from indicated RBBP7-high, or RBBP7-low BCa PDXs. **(J)** Representative whole lung and H&E graphs derived from mice treated with or without ORY-1001 in MCF-7-derived metastatic model. **(K)** Representative whole lung and H&E graphs derived from mice treated with or without ORY-1001 in MDA-MB-231-derived metastatic model. Data represent the Mean ± SD of at least three independent experiments. $^{*}P < 0.05$, $^{**}P < 0.01$, and $^{***}P < 0.001$. Differences were tested using a un-paired Student's t-test **(C**, **D**, **F**, **J**, **K)**, and the 2-way ANOVA followed by Tukey's multiple comparisons test **(H)**

expressed in breast cancer samples, relative to normal tissues. Kaplan-Meier analysis further showed that high RBBP7 correlated with poor prognosis of BCa individuals based on public GEO datasets. Our in vitro and in vivo xenograft tumor models further demonstrated that RBBP7 overexpression could facilitate tumor growth and distant lung metastasis. Mechanistically, we identified one specific super-enhancer, named RBBP7-SE, that contribute to driving high levels of RBBP7. Deletion of RBBP7-SE abrogated RBBP7 expressions and impaired the malignant progression of BCa cells. Furthermore, RBBP7 mainly activated the stemness-associated genes via recruiting LSD1. Therefore, we demonstrated that targeting LSD1 could effectively abolish the oncogenic effects of RBBP7 in BCa.

As a regulatory DNA sequence that mainly exists in non-coding regions, enhancers could remarkably elevate the transcriptional efficiency by interacting with adjacent promoters [27]. Containing high-density critical TFs and cofactors, super-enhancer (SE) belongs to specialized enhancer elements that forcefully augment the transcription of their target genes [28, 29]. Compared with typical enhancers, SE mainly possesses the following features: (1) TFs numbers and transcriptional activity of elements are much higher; (2) downstream genes driven by SE show much higher expressions; (3) SE preferentially recruits tissue-specific TFs to determine cell identity. As a result, we screened the high-throughput screening data of H3K27ac to find the RBBP7-SE has a larger binding size in MCF-7 cells, which is absent in normal MCF-10 A cells. Low-throughput ChIP-qPCR analysis further confirmed that RBBP7-SE depletion by CRISPR could substantially suppress the RBBP7 levels, showing the regulatory specificity of RBBP7-SE. The histone acetyltransferase CREB-binding protein (CBP) and its closely binding p300 proteins, defined as CBP/p300 complex, are indispensable for histone acetylation at enhancers, SE, and promoters. Along with RNA polymerase II and eRNA, CBP/p300 complexes are heavily enriched in SE regions to sustain chromatin accessibility and massive H3K27ac signals. Actually, CBP/P300 proteins adopt their intrinsic histone acetyltransferase (HAT) domain to maintain SE activity, which is the main factor for CBP/p300-dependent gene transcription. In line with the truth, targeting p300 via the siRNA method notably abolished H3K27ac enrichment on RBBP7-SE sites and subsequently inhibited RBBP7 levels. In addition, SE are reported to be commonly bound by BRD4 proteins that contribute to recruit Mediators and enrich chromatin modifiers. For instance, BRD4 is a master regulator of the transcriptional activation of ERα-occupied super-enhancers (ERSEs), potentiating ERα-induced gene transcriptional activation [30]. Given that SE is more likely to disrupt the expression transcription-regulating signature, targeting BRD4 via JQ1 was widely investigated and proved to be effective against SE-addicted tumors, like prostate cancer, neck squamous cell carcinoma, liver cancer, and ovarian cancer. In this study, we observed that JQ1 could inhibit RBBP7 expressions in a dose-dependent manner, suggesting that JQ1 administration may be an appropriate method to suppress RBBP7-driven BCa. Aberrant SE hijacking contributes to BCa growth, metastasis, or drug resistance, but relationships between SE assembly and BCa stemness maintenance were rarely reported. In this study, we identified a novel RBBP7-specific SE that could elevate RBBP7 levels to drive the stemness program. As a result, we could develop specific drugs to abrogate these SE elements, therefore effectively inhibiting BCa malignant phenotypes.

To further understand the stemness pathway epigenetically manipulated by RBBP7 in BCa, bioinformatics analysis was conducted and the self-renewal signal was intensively enriched in RBBP7-high BCa samples. Given that RBBP7 belongs to a subunit of the NuRD complex, we screened the other subunits that may contribute to RBBP7 functions in BCa. For instance, RUNX2 could recruit the NuRD(MTA1)/CRL4B complex to enhance breast cancer progression and bone metastasis [31]. Consistently, we screened that RBBP7-binding LSD1 may influence BCa stemness phenotypes. Mechanistically, RBBP7 recruits LSD1 to RBBP7-binding promoters of SOX2/SOX9/OCT4/CCND1, and LSD1 determined the transcriptional activation induced by RBBP7. Notably, LSD1 mediates the demethylation process of H3K9me3,

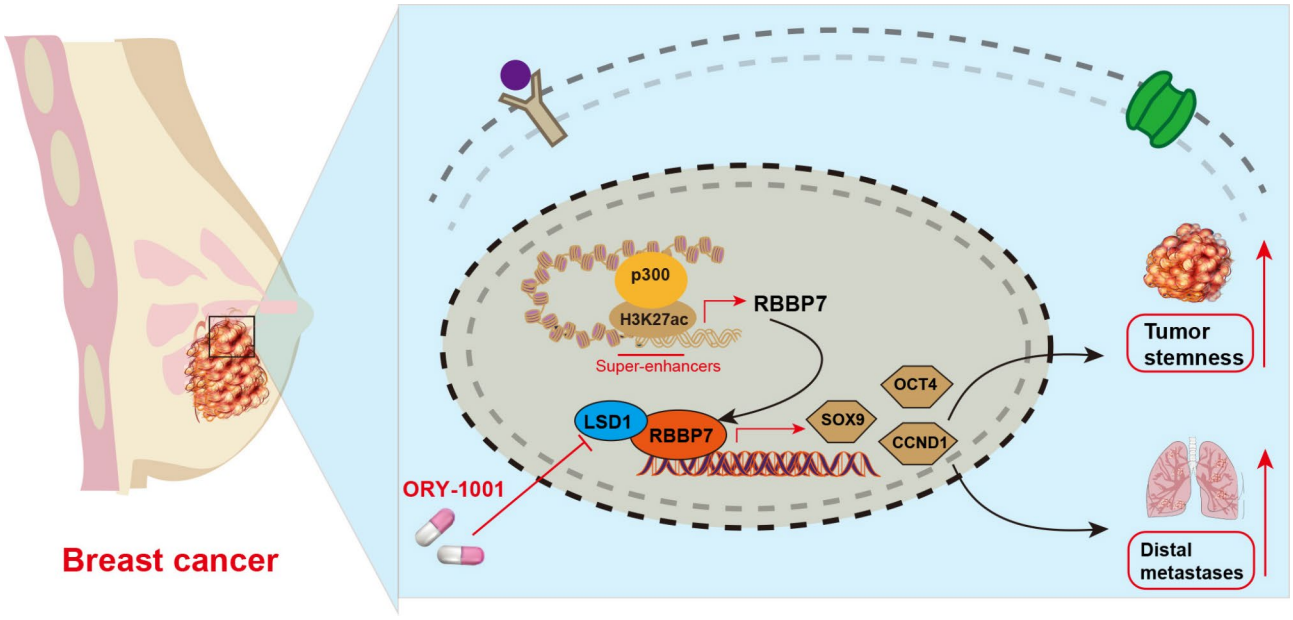

Fig. 8 Schematic illustration of the proposed model in which RBBP7-SE/RBBP7/LSD1 axis regulates tumor stemness and progression of BCa

which is a repressive histone modification. Similarly, LSD1 could up-regulate activating transcription factor 4 (ATF4) levels via erasing H3K9me2 and promoting glutathione (GSH) production during the progression of non-small cell lung cancer (NSCLC) [32]. Conversely, AMPK-mediated the phosphorylation of PHF2 to release the repressive H3K9me2, leading to limited lung cancer metastasis [33]. Furthermore, abnormal H3K9me2 modification levels correlate tightly with cancer stemness, like esophageal squamous cell carcinoma, colon cancer, as well as glioma [34–36]. We firstly confirmed the positive relationships between LSD1 and stemness-related signature in BCa, and mechanistic regulations were further clarified. RBBP7 depended on the epigenetic functions of LSD1 to activate stemness-related genes and sustained tumor growth, or migration. Therefore, we introduced the specific LSD1 inhibitor, ORY-1001, in BCa treatment. The dose-response curve suggested that ORY-1001 may possess remarkable inhibitory effects in RBBP7 high BCa cells, whereas it showed unsatisfactory efficiency in RBBP7^{low} cells. For these RBBP7^{low} BCa cells, ORY-1001 might lose effective targets. Therefore, tumor heterogeneity is an important factor thta affects the efficacy of ORY-1001. We further hypothesized that RBBP7-mediated LSD1 recruitment might be the essential step for LSD1-driven tumor growth. Thus, RBBP7 down-regulations or deficiency may compromise the LSD1 inhibitors. Besides, we demonstrated the in vitro findings in BCa patient-derived xenograft tumor models, where RBBP7-high PDXs were more sensitive to ORY-1001 than RBBP7-low PDXs. However, we failed to detect the impact of ORY-1001 on structures of RBBP7-SE in BCa. Considering that BCa metastasizes mainly through lymphatic or blood vessel metastasis, we demonstrated that ORY-1001 could effectively inhibit BCa lung metastasis, inducing negligible side effects.

Several limitations in this study deserve to be further resolved or improved. First, the prognostic significance of RBBP7 should be validated in more BCa samples from multi-center cohorts, not just the current public datasets. Secondly, Chromatin Immunoprecipitation sequencing (ChIP-seq) of H3K27ac/H3K4me1 in BCa cells should be performed to further investigate the structure and activity of RBBP7-SE. Thirdly, the relationships between RBBP7 and immune evasion in BCa, not only stemness maintenance, are still unknown. Last, we should discover the specific RBBP7 inhibitors for translational research, and the small molecular inhibitors targeting RBBP7 are currently still unavailable.

Conclusion

In conclusion, the present study reveals that the SE-hijacking RBBP7-mediated stemness pathway endows BCa with new epigenetic vulnerability. Abrogating the RBBP7-LSD1 complex may merit investigation as a therapeutic strategy for suppressing stemness and progression of BCa.

Supplementary Information

The online version contains supplementary material available at https://doi.org/10.1186/s12967-025-06270-3.

Supplementary Material 1: Figure S1. RBBP7 promotes BCa proliferation and migration in vitro. **(A)** RT-qPCR analysis and western blotting assays showing the RBBP7 overexpression in MDA-MB-231 and MDA-MB-453

cells. **(B)** RT-qPCR analysis and western blotting assays showing the RBBP7 inhibition in the indicated cells. **(C)** The representative EdU assays showing the proliferation rates in EV and RBBP7-overexpressing BCa cells. **(D-E)** Quantification of tumor weight of tumors derived from RBBP7-overexpressing **(D)** or RBBP7-KD cells **(E)**. **(F-G)** Transwell assays and quantification data in RBBP7-overexpressing **(F)** or RBBP7-KD cells **(G)**.

Supplementary Material 2: Figure S2. RBBP7 relies on LSD1 to regulate stemness-related signature. **(A-B)** Luciferase assays showing the relative trans-activation activities of the promoters of the four genes in RBBP7-overexpressing (A) or RBBP7-KD (B) cells. **(C)** RT-qPCR analysis showing relative mRNA levels of stemness-reelated signature in cells transfected with indicated siRNAs. **(D)** ChIP-qPCR analysis showing the relative levels of Ser5- and Ser2-phosphorylated RNA Pol II CTDs in promoters of indicated genes in RBBP7-KD cells with or without RBBP7 restoration. **(E)** CCK-8 assays showing the relative cells growth in cells with or without LSD1 inhibition. **(F-G)** Colony formation or Transwell asssays showing the growth or migration abilities in cells with or without LSD1 inhibition

Supplementary Material 3: Figure S3. Quantification of pharmaceutical effects of ORY-1001 in treating BCa. **(A)** Quantification of tumor weight in the indicated mice treated with or without ORY-1001. **(B)** Comparison of hematological parameters in mice treated with or without ORY-1001. **(C)** H&E slides of organ tissues in the indicated mice treated with or without ORY-1001

Acknowledgements
None.

Author contributions
Ying Hu, Jun Jiang, and Peng Tang designed the project and assays. Yuanyin Xi Ruoding Wang, and Man Qu conducted the experimental assays. Qinwen Pan, and Minghao Wang conducted the bioinformatic and statistical analysis. Xiang Ai, Chao and Zihan Sun collected the melanoma tissues. Ying Hu wrote the paper and Jun Jiang revised it. All authors have approved the final manuscript.

Funding
None.

Data availability
The data used to support the findings of this study are available from the corresponding author upon request. The public BRCA patient dataset was obtained from the Cbioportal website (https://www.cbioportal.org/) and Kaplan-Meier Plotter (https://kmplot.com/analysis/index.php?p=service).

Declarations

Ethics approval and consent to participate
The study was reviewed and approved by the Southwest Hospital, Army Medical University, Chongqing, China.

Consent for publication
Not applicable.

Competing interest
The authors declare that the research was conducted in the absence of any commercial or financial relationships that could be construed as a potential conflict of interest.

Author details
[1]Department of Thyroid and Breast Surgery, Southwest Hospital, Army Medical University, Chongqing, China
[2]Department of Clinical Laboratory Medicine, Southwest Hospital, Army Medical University, Chongqing, China
[3]Department of Thyroid and Breast Surgery, The General Hospital of Western Theater Command, Chengdu 610083, China
[4]Breast Disease Center, Guiqian International General Hospital, Guiyang, China
[5]Department of Breast, Thyroid and Vascular Surgery, Chongqing University FuLing Hospital, Chongqing University, Chongqing 402774, China

Received: 22 August 2024 / Accepted: 19 February 2025
Published online: 04 March 2025

References

1. Siegel RL, Giaquinto AN, Jemal A. Cancer statistics, 2024. CA Cancer J Clin. 2024;74(1):12–49.
2. Yang F, Xiao Y, Ding J-H, Jin X, Ma D, Li D-Q et al. Ferroptosis heterogeneity in triple-negative breast cancer reveals an innovative immunotherapy combination strategy. Cell Metab. 2023;35(1).
3. Geng S-Q, Alexandrou AT, Li JJ. Breast cancer stem cells: multiple capacities in tumor metastasis. Cancer Lett. 2014;349(1):1–7.
4. Lee RS, Sad K, Fawwal DV, Spangle JM. Emerging role of epigenetic modifiers in breast cancer pathogenesis and therapeutic response. Cancers (Basel). 2023;15(15).
5. Thakur C, Qiu Y, Pawar A, Chen F. Epigenetic regulation of breast cancer metastasis. Cancer Metastasis Rev. 2024;43(2):597–619.
6. Fitz-James MH, Cavalli G. Molecular mechanisms of transgenerational epigenetic inheritance. Nat Rev Genet. 2022;23(6):325–41.
7. Zhou L, Ng DS-C, Yam JC, Chen LJ, Tham CC, Pang CP, et al. Post-translational modifications on the retinoblastoma protein. J Biomed Sci. 2022;29(1):33.
8. Nabeel-Shah S, Garg J, Saettone A, Ashraf K, Lee H, Wahab S, et al. Functional characterization of RebL1 highlights the evolutionary conservation of oncogenic activities of the RBBP4/7 orthologue in Tetrahymena thermophila. Nucleic Acids Res. 2021;49(11):6196–212.
9. Moody RR, Lo M-C, Meagher JL, Lin C-C, Stevers NO, Tinsley SL, et al. Probing the interaction between the histone Methyltransferase/deacetylase subunit RBBP4/7 and the transcription factor BCL11A in epigenetic complexes. J Biol Chem. 2018;293(6):2125–36.
10. Li J, Zheng H, Hou J, Chen J, Zhang F, Yang X et al. X-linked RBBP7 mutation causes maturation arrest and testicular tumors. J Clin Invest. 2023;133(20).
11. Fang Y, Tang W, Qu S, Li Z, Zhang X, Miao Y, et al. RBBP7, regulated by SP1, enhances the Warburg effect to facilitate the proliferation of hepatocellular carcinoma cells via PI3K/AKT signaling. J Transl Med. 2024;22(1):170.
12. Wang J, He C, Gao P, Wang S, Lv R, Zhou H, et al. HNF1B-mediated repression of SLUG is suppressed by EZH2 in aggressive prostate cancer. Oncogene. 2020;39(6):1335–46.
13. Thakur A, Rahman KW, Wu J, Bollig A, Biliran H, Lin X, et al. Aberrant expression of X-linked genes RbAp46, Rsk4, and Cldn2 in breast cancer. Mol Cancer Res. 2007;5(2):171–81.
14. Lee SY, Jeong EK, Ju MK, Jeon HM, Kim MY, Kim CH, et al. Induction of metastasis, cancer stem cell phenotype, and oncogenic metabolism in cancer cells by ionizing radiation. Mol Cancer. 2017;16(1):10.
15. Taurin S, Alkhalifa H. Breast cancers, mammary stem cells, and cancer stem cells, characteristics, and hypotheses. Neoplasia. 2020;22(12):663–78.
16. Lawson DA, Bhakta NR, Kessenbrock K, Prummel KD, Yu Y, Takai K, et al. Single-cell analysis reveals a stem-cell program in human metastatic breast cancer cells. Nature. 2015;526(7571):131–5.
17. Luo M, Bao L, Xue Y, Zhu M, Kumar A, Xing C et al. ZMYND8 protects breast cancer stem cells against oxidative stress and ferroptosis through activation of NRF2. J Clin Invest. 2024;134(6).
18. Zhang J, Hu Z, Chung HH, Tian Y, Lau KW, Ser Z, et al. Dependency of NELF-E-SLUG-KAT2B epigenetic axis in breast cancer carcinogenesis. Nat Commun. 2023;14(1):2439.
19. Sachamitr P, Ho JC, Ciamponi FE, Ba-Alawi W, Coutinho FJ, Guilhamon P, et al. PRMT5 Inhibition disrupts splicing and stemness in glioblastoma. Nat Commun. 2021;12(1):979.
20. Dong J, Li J, Li Y, Ma Z, Yu Y, Wang C-Y. Transcriptional super-enhancers control cancer stemness and metastasis genes in squamous cell carcinoma. Nat Commun. 2021;12(1):3974.
21. Chow P-M, Chang Y-W, Kuo K-L, Lin W-C, Liu S-H, Huang K-H. CDK7 Inhibition by THZ1 suppresses cancer stemness in both chemonaïve and chemoresistant urothelial carcinoma via the Hedgehog signaling pathway. Cancer Lett. 2021;507:70–9.
22. Niu M, Yi M, Wu Y, Lyu L, He Q, Yang R, et al. Synergistic efficacy of simultaneous anti-TGF-β/VEGF bispecific antibody and PD-1 Blockade in cancer therapy. J Hematol Oncol. 2023;16(1):94.
23. Lee SH, Hu W, Matulay JT, Silva MV, Owczarek TB, Kim K et al. Tumor evolution and drug response in Patient-Derived organoid models of bladder Cancer. Cell. 2018;173(2).

24. Keck KM, Pemberton LF. Histone chaperones link histone nuclear import and chromatin assembly. Biochim Biophys Acta. 2013;1819(3–4):277–89.
25. Xiao L, Dang Y, Hu B, Luo L, Zhao P, Wang S, et al. Overlapping functions of RBBP4 and RBBP7 in regulating cell proliferation and histone H3.3 deposition during mouse preimplantation development. Epigenetics. 2022;17(10):1205–18.
26. Guo L, Xia Y, Li H, Wang Z, Xu H, Dai X, et al. FIT links c-Myc and P53 acetylation by recruiting RBBP7 during colorectal carcinogenesis. Cancer Gene Ther. 2023;30(8):1124–33.
27. Schoenfelder S, Fraser P. Long-range enhancer-promoter contacts in gene expression control. Nat Rev Genet. 2019;20(8):437–55.
28. Pott S, Lieb JD. What are super-enhancers? Nat Genet. 2015;47(1).
29. Tang F, Yang Z, Tan Y, Li Y. Super-enhancer function and its application in cancer targeted therapy. NPJ Precis Oncol. 2020;4:2.
30. Zheng Z-Z, Xia L, Hu G-S, Liu J-Y, Hu Y-H, Chen Y-J, et al. Super-enhancer-controlled positive feedback loop BRD4/ERα-RET-ERα promotes ERα-positive breast cancer. Nucleic Acids Res. 2022;50(18):10230–48.
31. Yin X, Teng X, Ma T, Yang T, Zhang J, Huo M, et al. RUNX2 recruits the NuRD(MTA1)/CRL4B complex to promote breast cancer progression and bone metastasis. Cell Death Differ. 2022;29(11):2203–17.
32. Du L, Yang H, Ren Y, Ding Y, Xu Y, Zi X, et al. Inhibition of LSD1 induces ferroptosis through the ATF4-xCT pathway and shows enhanced anti-tumor effects with ferroptosis inducers in NSCLC. Cell Death Dis. 2023;14(11):716.
33. Dong Y, Hu H, Zhang X, Zhang Y, Sun X, Wang H, et al. Phosphorylation of PHF2 by AMPK releases the repressive H3K9me2 and inhibits cancer metastasis. Signal Transduct Target Ther. 2023;8(1):95.
34. Jia R, Yang L, Yuan X, Kong J, Liu Y, Yin W, et al. GASC1 promotes stemness of esophageal squamous cell carcinoma via NOTCH1 promoter demethylation. J Oncol. 2019;2019:1621054.
35. Bergin CJ, Zouggar A, Haebe JR, Masibag AN, Desrochers FM, Reilley SY, et al. G9a controls pluripotent-like identity and tumor-initiating function in human colorectal cancer. Oncogene. 2021;40(6):1191–202.
36. Tao H, Li H, Su Y, Feng D, Wang X, Zhang C, et al. Histone methyltransferase G9a and H3K9 dimethylation inhibit the self-renewal of glioma cancer stem cells. Mol Cell Biochem. 2014;394(1–2):23–30.

Publisher's note